Southern Annular Mode drives multicentury wildfire activity in southern South America

Andrés Holz[a,1], Juan Paritsis[b], Ignacio A. Mundo[c,d], Thomas T. Veblen[e], Thomas Kitzberger[b], Grant J. Williamson[f], Ezequiel Aráoz[g], Carlos Bustos-Schindler[h], Mauro E. González[h,i], H. Ricardo Grau[g,j], and Juan M. Quezada[k]

[a]Department of Geography, Portland State University, Portland, OR 97207; [b]Laboratorio Ecotono, Instituto de Investigaciones en Biodiversidad y Medioambiente, Consejo Nacional de Investigaciones Científicas y Técnicas, Universidad Nacional del Comahue, 8400 Bariloche, Argentina; [c]Laboratorio de Dendrocronología e Historia Ambiental, Instituto Argentino de Nivología, Glaciología y Ciencias Ambientales, El Centro Científico Tecnológico, Consejo Nacional de Investigaciones Científicas y Técnicas, M5502IRA Mendoza, Argentina; [d]Facultad de Ciencias Exactas y Naturales, Universidad Nacional de Cuyo, M5502JMA Mendoza, Argentina; [e]Department of Geography, University of Colorado, Boulder, CO 80309; [f]School of Biological Sciences, University of Tasmania, Hobart, TAS 7001, Australia; [g]Instituto de Ecología Regional, Consejo Nacional de Investigaciones Científicas y Técnicas, Universidad Nacional de Tucumán, 4172 Yerba Buena, Argentina Argentina; [h]Instituto de Conservación, Biodiversidad y Territorio, Facultad de Ciencias Forestales y Recursos Naturales, Instituto de Silvicultura, Universidad Austral de Chile, Valdivia, Chile; [i]Center for Climate and Resilience Research (CR2), Santiago, Chile; [j]Facultad de Ciencias Naturales e Instituto Miguel Lillo, Universidad Nacional de Tucumán, 4000 San Miguel de Tucumán, Argentina; and [k]Facultad de Ciencias Forestales, Universidad Nacional de Misiones, Eldorado, 3380 Misiones, Argentina

Edited by Glen M. MacDonald, University of California, Los Angeles, CA, and approved July 24, 2017 (received for review April 1, 2017)

The Southern Annular Mode (SAM) is the main driver of climate variability at mid to high latitudes in the Southern Hemisphere, affecting wildfire activity, which in turn pollutes the air and contributes to human health problems and mortality, and potentially provides strong feedback to the climate system through emissions and land cover changes. Here we report the largest Southern Hemisphere network of annually resolved tree ring fire histories, consisting of 1,767 fire-scarred trees from 97 sites (from 22 °S to 54 °S) in southern South America (SAS), to quantify the coupling of SAM and regional wildfire variability using recently created multicentury proxy indices of SAM for the years 1531–2010 AD. We show that at interannual time scales, as well as at multidecadal time scales across 37–54 °S, latitudinal gradient elevated wildfire activity is synchronous with positive phases of the SAM over the years 1665–1995. Positive phases of the SAM are associated primarily with warm conditions in these biomass-rich forests, in which widespread fire activity depends on fuel desiccation. Climate modeling studies indicate that greenhouse gases will force SAM into its positive phase even if stratospheric ozone returns to normal levels, so that climate conditions conducive to widespread fire activity in SAS will continue throughout the 21st century.

fire scars | climate modes | AAO | synchrony | warming

Fire is a key ecological process in southern South America (SSA) that affects ecosystem dynamics and services (1) and smoke-related human health (2). Fire activity in SSA is driven primarily by variations in fuel amount and condition, ignition patterns, and climate variability (3, 4). In SSA, wildfire activity is related to large-scale climate modes, such as the El Niño-Southern Oscillation (ENSO), as evidenced in landscape-scale tree ring fire histories typically spanning ∼2° of latitude (5–7) and in modern documentary fire records across biomes ranging from semiarid to rainforest ecosystems (3). Understanding fire–climate relationships can clarify the relative importance of humans in either increasing or decreasing wildfire activity, and help land managers better anticipate future fire activity under climate change (3). To date, however, there have been no broad-scale syntheses of long-term (i.e., multicentury) fire activity and climate–fire dynamics for any region in the Southern Hemisphere.

Since the 1950s, there has been a rise in temperature during the growing season at mid to high latitudes in the Southern Hemisphere (Fig. 1*A*), a phenomenon largely attributed to an intensification and poleward shift in the Southern Hemisphere westerlies- associated variability of the Southern Annular Mode (SAM) (8–11) (Fig. 1*B*). During this period, the SAM has experienced an upward (positive) trend during spring and summer (Fig. 1*C*), attributed to stratospheric ozone depletion and increases in greenhouse gases (12), which is unprecedented over the last 1,000 y (13). The leading pattern of tropospheric circulation variability south of 20 °S, the SAM is essentially a zonally symmetric or annular structure with synchronous, seesaw-like anomalies of opposite signs in Antarctica and the midlatitudes (∼40–50°S) (8). During the SAM's positive phase, decreased (increased) surface pressure and geopotential heights are observed over Antarctica (midlatitudes) and the southern westerly winds strengthen and shift poleward, while opposite conditions prevail during its negative phase (8, 14). For SSA, this SAM-mediated increase in surface pressure and geopotential heights acts like a blocking pressure system that since the 1950s has been associated with (*i*) warmer conditions due to a combination of enhanced horizontal advection, subsidence, and solar radiation (15), particularly south of 40 °S and during the summer (14), and (*ii*) dry conditions due to reduced frontal and orographic precipitation (16) and weakening of the moisture convergence (17), particularly at 40°S and in the spring (14).

The SAM has been shown to be a major driver of fire activity across the broad range of ecosystem types, from semiarid to rainforest ecosystems, based on short (1984–2010) documentary fire records (3) and over a centennial time scale (ca. 1800 to the

Significance

Fire is a key ecological process affecting ecosystem dynamics and services, driven primarily by variations in fuel amount and condition, ignition patterns, and climate. In the Southern Hemisphere, current warming conditions are linked to the upward trend in the Southern Annular Mode (SAM) due to ozone depletion. Here we use tree ring fire scar data obtained from diverse biomes ranging from subtropical dry woodlands to sub-Antarctic rainforests to assess the effect of the SAM on regional fire activity over the past several centuries. Our findings reveal a tight coupling between fire activity and the SAM at all temporal scales and in all biomes, with increased wildfire synchrony and activity during the 20th century compared with previous centuries.

Author contributions: A.H., J.P., and T.T.V. designed research; A.H. performed research; A.H., T.T.V., and G.J.W. analyzed data; A.H., J.P., I.A.M., T.T.V., T.K., E.A., C.B.-S., M.E.G., H.R.G., and J.M.Q. provided fire scar data and A.H., J.P., I.A.M., T.T.V., and T.K. interpreted results; and A.H. and T.T.V. led the writing of the paper, and all authors contributed substantially to revisions.

The authors declare no conflict of interest.

This article is a PNAS Direct Submission.

Data deposition: The tree-ring fire scar data reported in this paper have been deposited in the International Tree-Ring Data Bank (ITRDB), https://www.ncdc.noaa.gov/data-access/paleoclimatology-data/datasets/tree-ring.

[1]To whom correspondence should be addressed. Email: andres.holz@pdx.edu.

This article contains supporting information online at www.pnas.org/lookup/suppl/doi:10.1073/pnas.1705168114/-/DCSupplemental.

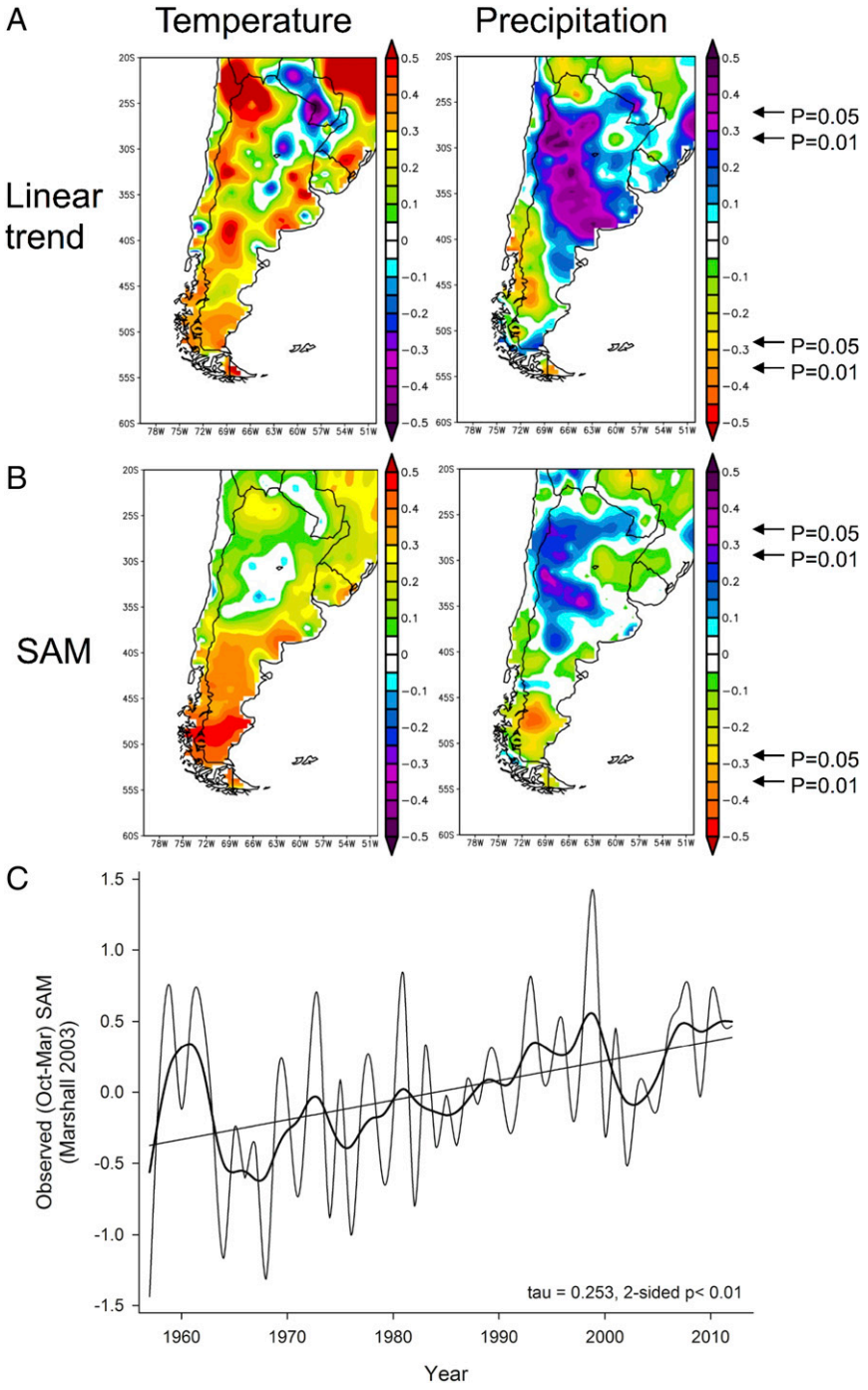

Fig. 1. Modern trends and teleconnections of climate and the SAM in SSA. (*A* and *B*) Spatial correlation between observed precipitation and temperature (gridded July–February data; University of Delaware) with a linear time series (i.e., 1, 2, 3. . .) for the 1949–2008 period (*A*) and observed (July–February) SAM for the 1957–2008 period (*B*). (*C*) Mean spring–summer (October–March) values of the observed SAM for 1957–2012 (9, 12); www.nerc-bas.ac.uk/icd/gjma/sam.html. Significant correlation (P <0.05 and <0.01) are indicated with arrows in *A* and *B*. In *C*, a linear fit and low-pass Gaussian filter (bold line) highlight the low-frequency trend (11-y window), and values for Kendall's τ statistic and two-sided P values are shown. The series was also tested for lag-1 correlation, which was found to be nonsignificant ($P > 0.05$).

present) for specific forest types based on tree ring fire histories (7, 18). However, we lack a comprehensive understanding of the SAM's influence on fire activity over multiple centuries and at a broad latitudinal extent of forest ecosystems in SSA. We hypothesize that in biomass-rich temperate forests extending from ~37° to 55° S in SSA, the SAM promotes fire primarily by enhancing warm spring-summer conditions, which in turn desiccate fuels. Here we used 4,587 annually resolved fire scar dates from 1,767 fire-scarred trees collected at 97 sites (the largest paleofire record yet assembled for the Southern Hemisphere) to reconstruct regional fire records for eight regions that extend from subtropical to sub-Antarctic latitudes in SSA and span the period 990–2010 AD (Fig. 2*A* and *SI Appendix*, Fig. S1 and Table S1). From these fire scar dates, we developed indices of regional- and subcontinental-scale fire activity and synchrony to examine relationships between the SAM and local and regional climate parameters across SSA at

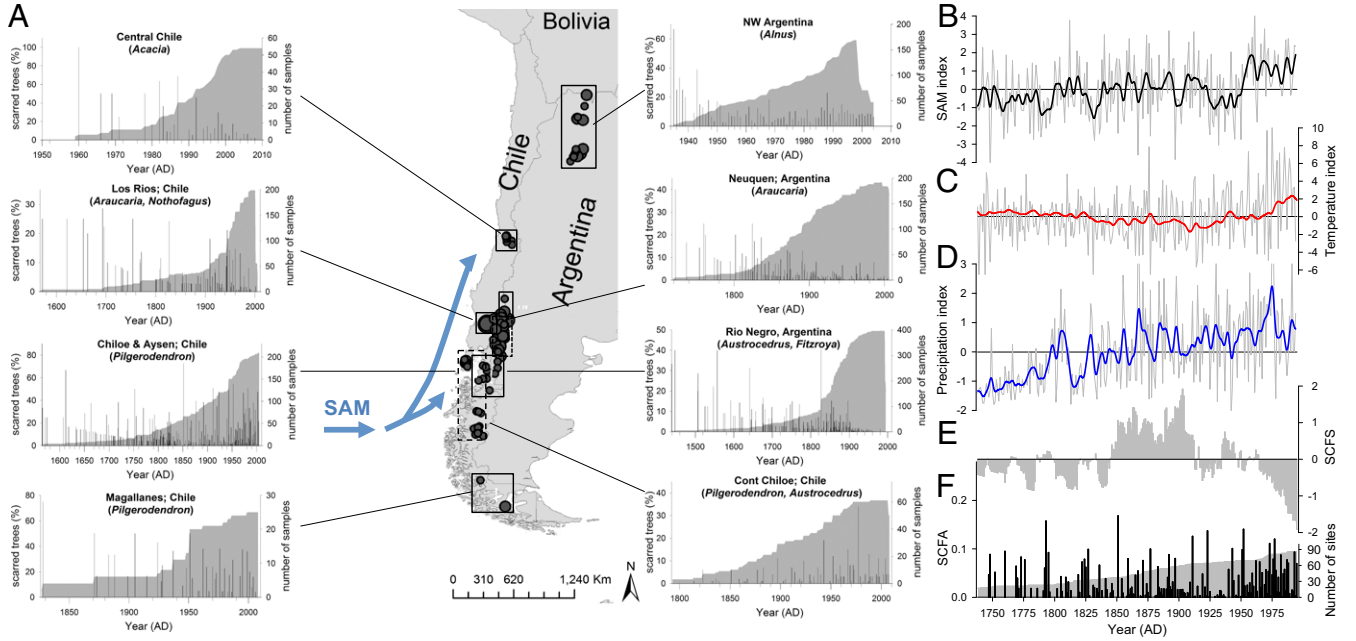

Fig. 2. Tree ring-based fire history and study regions (97 sites and 1,767 fire scars) in SSA. Study region locations (boxes) and primary sampled species (in parentheses) are indicated. Histograms show the fire-scarred trees (%; vertical bars on the left *y* axis) and sample depth (gray area on the right *y* axis; starting when ≥3 trees per region had been scarred at least once); note that the *x*- and *y*-axes are not scaled equally in each region (*A*). Light-blue arrows indicate the geographical domain of the dominant extratropical forcing of regional climate variability, as represented by the SAM. The number of sites sampled within each region is indicated by the size of the black circles on the map. Graphs in the far right column show reconstruction of the SAM index departures (December–February; Marshall, black line) (26) (*B*), temperature departures (mean annual reconstruction for the Southern Hemisphere; red line) (28) (*C*), precipitation departures (total December–February SSA reconstruction; blue line) (27) (*D*), SCFS departures (gray bars; 15-y moving averages) (*E*), and SCFA (black bars) and total number of search sites (i.e., sample depth; gray fill) (*F*). All climate series and the SCFS were standardized (*z*-scores, in SD units), detrended, and prewhitened. All annually resolved climate series (light-gray lines) were smoothed with a 15-y spline. Records from northwestern Argentina and central Chile were not used in building the subcontinental fire indices owing to their short sample depth.

multiple time scales. Our rationale is that at the regional and subcontinental scales, high synchrony indicates a strong influence of climatic variations on fire (19), and that overall high fire activity could have a strong association with climate variability (19–21) as well as with changes in ignition owing to either natural (22) or human (23–25) causes.

We used a recently developed proxy reconstruction of summer (December–February) SAM (9, 26) to examine the relation of fire activity to variability in the SAM (*Methods*). This SAM reconstruction has proven useful in explaining tree growth variability in much of our study area (26). We also tested for the influence of variabilities in precipitation and temperature on fire activity at multiple scales, using proxy reconstructions of precipitation for SSA (27) and of temperature for the Southern Hemisphere (precipitation index and temperature index hereinafter) that are heavily weighted by the Pacific sector of the Southern Hemisphere and thus suitable for our study area (28).

Results and Discussion

Reconstructed mean values of the SAM during years of widespread fire (no fire) are significantly above (significantly or trend below) the long-term mean in all study regions located south of 37°S (*SI Appendix*, Figs. S2 and S3 and Text ST1). During the period of the instrumental records (1957–2013), higher (lower) SAM values are correlated with higher (lower) temperatures and reduced (increased) precipitation in most seasons of the year, including the fire season (*SI Appendix*, Fig. S4). In all study regions south of 37 °S in SSA, the overall pattern is one of increased fire activity driven by fuel desiccation, rather than by insufficient quantity of fine fuel (*SI Appendix*, Text ST1), associated with a positive SAM, which closely coincides with and is supported by results and interpretations from modern burned area–climate relationships in woody vegetation over the 1984–2010 period (3).

The collective fire history of all study regions' chronologies south of 37 °S combined (minimum of two trees and 10% of recorder trees per site) shows a rapid decline from early in the record (1400s) to the 1700s, when fire activity increased gradually (*SI Appendix*, Fig. S1). Starting in the 1850s, fire activity increased very abruptly, and large fire years occurred roughly every 15–20 y until the 1920–1940s, when fire activity dropped. Starting in the 1960s, fire activity ramped up again and has continued to the present day (*SI Appendix*, Fig. S1). The temporal pattern of the collective fire history of all regions is similar to the standardized synthesis of all charcoal records located south of 30 °S in western South America (29). The post-1960s increases in fire activity has been driven primarily by fire activity at mid and high latitudes on the west side of the Andes (Fig. 2*A*), where wildfires on the eastern Andean slope show the effects of active fire suppression since the 1930s–40s (Fig. 2*A*). The subcontinental-scale fire indices indicate that both the magnitude of fire activity (SCFA) and fire synchrony (SCFS) among regions have fluctuated over time and that in general there is no clear relationship between these two indices (Fig. 2 *E* and *F*). In contrast to the SCFA index, the amplitude in the SCFS index has increased over time, with higher maximum values and lower minimum values in the latter part of the analyzed period (1738–1932) compared with early in the record.

Relatively weak but significant correlations were found for both subcontinental fire indices (SCFA: $r = 0.2$, $P < 0.01$; SCFS: $r = 0.18$, $P < 0.01$) and the SAM during the 1738–1932 period (Table 1). Series were prewhitened to remove autocorrelation, and the trend-free records were filtered with a 15-y spline to match the main spectra of the SCFA (*SI Appendix*, Fig. S5). Likewise, similar low-frequency variability patterns were shared between the temperature

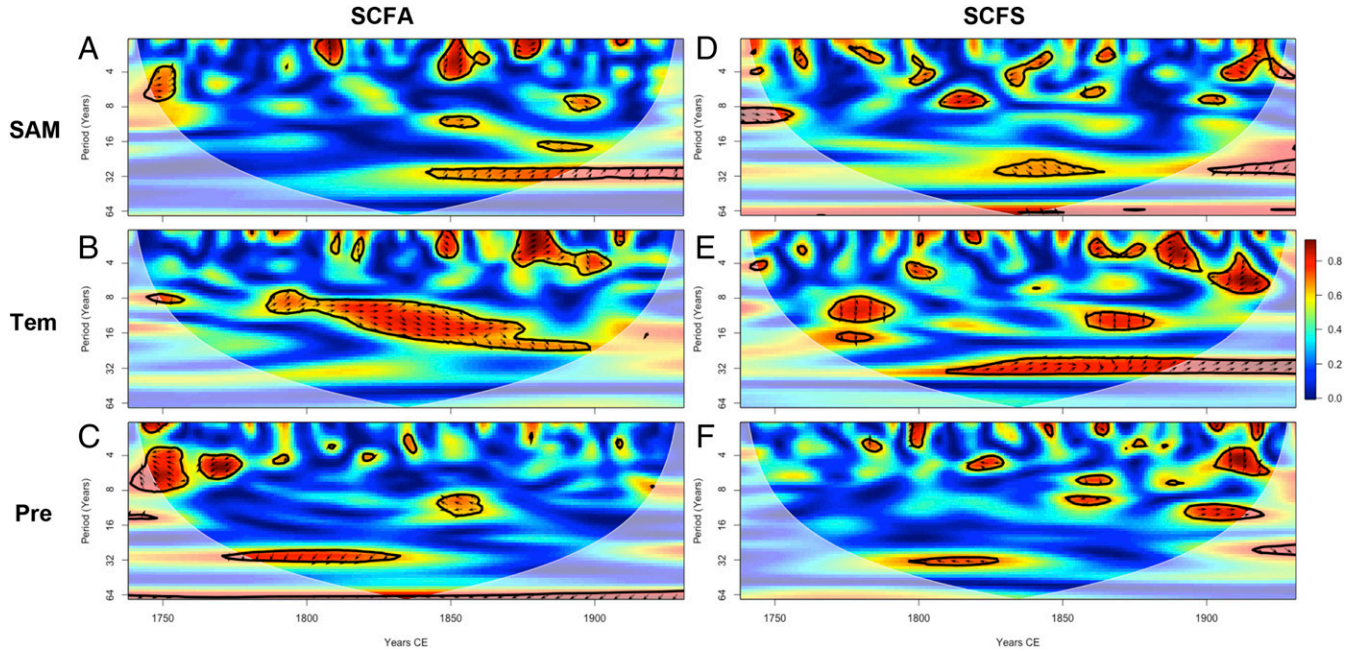

Fig. 3. Wavelet coherence between climate and fire at the subcontinental scale (SCFA, *Left*, and SCFS, *Right*) and SAM (*A* and *D*) temperature (*B* and *E*), and precipitation (*C* and *F*) index reconstructions. Red regions in the plots indicate the frequencies and times for which pairs of series were coherent. The cone of influence (white dashed line) and the significant coherent time-frequency regions ($P < 0.01$; 1,000 Monte Carlo simulations; black solid line) are indicated. All figures were computed using standardized (i.e., *z*-scores) series that were detrended and prewhitened (*Methods*). Data sources: SAM (December–February), (9); temperature index (mean annual reconstruction for the Southern Hemisphere), (28); precipitation index (total December–February SAS reconstruction), (27).

and SCFA indices ($r = 0.12$, $P < 0.01$) and between the precipitation and SCFS indices ($r = 0.24$, $P < 0.01$) (Table 1).

The patterns of wavelet coherence between the SCFA and both the SAM and temperature indices show numerous shorter (ca. four 2–8 y) and longer (ca. two 10–18 y) periods with either in-phase and/or delayed in-phase coherence throughout the recording period (Fig. 3 *A* and *B* and *SI Appendix*, Text ST1). Similarly, the SCFS and SAM indices share similar common numerous short (ca. 4–8 y) and a few longer (ca. 8–12-y) periods with either in-phase and/or delayed in-phase coherence (Fig. 3*D*). Some of the short period coherence might reflect the linkage of fire and the climatic parameters to ENSO variability documented in previous studies (5–7, 30, 31); however, the goal of the present analysis was to identify the SAM signal in the coherence patterns. Only decadal-scale in-phase and/or delayed in-phase coherence (ca. 28–34 y) is shared between SCFS and temperature (Fig. 3*E*). The precipitation index and both fire indices share mostly antiphase or delayed antiphase coherence (i.e., drought and fire), with common numerous short (ca. 1–8 y) and fewer longer (ca. 8–10 y) periods (Fig. 3 *C* and *F*). Precipitation also shares a few common in-phase and/or delayed in-phase coherence of longer (ca. 10–16 y) periods with the SCFS (Fig. 3*F*). Overall, wavelet coherence analyses on the SCFA also show a predominant role of drought in the first third of the record (i.e., 1738–1825), with the SAM and temperature indices increasing in relevance over the remaining record (Fig. 3 *A*–*C*). Similarly, an increase in coherence between the precipitation and SCFS indices is also observed from the 1780s to 1930s (Fig. 3*F*), but no obvious change in coherence over time is noted between the SCFS and either the SAM or temperature index (Fig. 3 *D* and *E*).

The foregoing results indicate that at the subcontinental-scale, large wildfire years (SCFA) were driven primarily by warm conditions teleconnected with a positive SAM during 1738–1932. Some years of high synchrony in subcontinental fire activity are linked to reduced rainfall. In both cases, our rationale in interpreting these results is that in SSA [and elsewhere (19, 20, 32)], large fire years in cool and/or wet forests with abundant fuels and a short fire season have been commonly associated with periods of warm and dry conditions that reduce fuel moisture and favor fire activity. We speculate that the association between high fire synchrony and above-average precipitation reflects the spread of fires that began in fuel-limited grasslands adjacent to the core areas sampled for fire scars, where previous research had shown a lagged association of fire and fine fuel-enhancing moister conditions (5, 33). This interpretation is consistent with the lagged association of fire with above-average moisture availability in grassland habitats throughout SSA based on modern climate-fire analyses using instrumental climate records and observations of annual area burned (3).

The peaks in fire activity in the mid-1800s and early 1900s have been linked to coincident increases in human-set fires and climate variability in some of our study regions (6, 34, 35). While increases in fire frequencies in association with the increased presence of

Table 1. Pearson correlation values of 15-y smoothed time series (z-scores) of climate and fire (SCFA and SCFS) over the 1738–1932 period (n = 194)

Series	*r* value
SCFA vs. SAM	0.20***
SCFA vs. temperature	0.12*
SCFA vs. precipitation	−0.09
SCFS vs. SAM	0.18**
SCFS vs. temperature	−0.05
SCFA vs. precipitation	0.24***
SCFA vs. SCFS	0.07

All reconstructions were filtered with a 15-y spline to emphasize the correlations among the low frequency of all records. All time series were detrended. Pearson correlation coefficients were calculated from prewhitened series using the trend-free prewhitening procedure in the zyp R package. The subcontinental fire indices were built using a constant number of fire recording sites over the 1738–1932 period. *$P < 0.05$; **$P < 0.01$; ***$P < 0.001$.

indigenous and modern humans are detectable in specific habitats, periods of synchronous widespread fire documented at annual resolution in tree ring studies and at multidecadal resolution in sedimentary charcoal studies have been more strongly linked to climatic variability (4, 6, 34). Human amplification or dampening of climate-induced trends in wildfire activity would not have been synchronous across the six study areas, given different time periods of migrations of indigenous populations and colonization by populations of European origin until the 1930s–1940s, when fire records in some regions clearly reflect fire exclusion (e.g., ref. 7), but records in other regions reflect increased burning by modern humans (34). Thus, we use 1932 as a cutoff to reduce the impact of modern changes in human ignition (Fig. 2 *A* and *F* and *Methods*) while acknowledging that in some regions, pre-1932 human amplification and/or changes in lightning activity (1, 36) might have affected both subcontinental-scale indices (SCFA and SCFS).

Conclusions and Implications

In SSA, wildfire activity is strongly associated with warm conditions teleconnected with positive a SAM at multiple time scales both within large areas defined by specific forest ecosystem types and at subcontinental scales across a broad range of forest ecosystem types. At an interannual time scale, widespread fires across SSA co-occurred during anomalously high SAM conditions over an extensive north-to-south gradient at ∼37–54°S, based on 1,252 scarred trees at 71 sites. Across this latitudinal range, most study sites are dominated by forests ranging from moderate- to high-density stands in which fuel quantity is not limiting to fire occurrence and instead years of widespread fire depend on fuel desiccation (*SI Appendix*, Text ST1). Ice cores and other proxies from Antarctica and SSA show that the positive trend in the SAM since the 1940s is at its highest level over at least the past 1,000 y (13), and that atmospheric greenhouse gases will keep forcing the SAM into its positive phase even if stratospheric ozone returns to normal levels (12, 37). Atmospheric greenhouse gases are also expected to force more frequent extreme El Niño events (38), which have been shown to be strongly associated with years of large wildfire activity in SSA (mainly north of 44°S) both directly and in combination with a positive SAM at the intraregional scale (*SI Appendix*, Tables S2 and S4). During the 2016–17 fire season, more than 500,000 hectares affected in the zone between ∼29 °S and 40 °S (∼3–5% of only that latitudinal zone) were burned in central and southern Chile, driven by a long-lasting drought that was amplified by concurrent positive SAM and ENSO conditions. While wildfire activity is expected to continue to reflect interannual variability related to ENSO, the continued dominance of the SAM as the primary driver of extratropical climate variability in the Southern Hemisphere (11, 37) portends increased wildfire activity in SSA for the 21st century.

Methods

Study Sites and Species. Tree ring fire scar records were obtained from the International Multiproxy Paleofire Database (IMPD), and from published and unpublished sources (*SI Appendix*, Table S1). This dataset consists of 1,767 fire-scarred trees from 97 sites in SSA extending from northwestern Argentina to southern Patagonia, which were grouped into eight regions of homogeneous climate variability (Fig. 2*A*) (following ref. 3). Included ecosystems range from relatively dry woodlands and forests to mesic and rain forests and bogs.

Indices. We created regional- and subcontinental-scale indices of years of fire activity to highlight and test for changes at interannual and decadal scales. Annual indices of fire occurrence (i.e., fire index) were calculated for each of the 97 sites by dividing the number of fire-scarred trees per year (with a minimum of two) by the number of trees potentially recording fire in that year, as described previously (24, 39). The start and end dates for each site fire index were determined using a minimum of four samples capable of recording fire. A region-wide fire index (for each of our eight regions) was then calculated as the sum of the site indices per year divided by the number of sites recording fire in that year (*SI Appendix*, Table S3). The SCFA was then calculated as the sum of the regional fire indices per year divided by the number of regions recording fire in that year (Fig. 2*F*).

For the SCFS, in a modification of a previously described method (19), annual fire synchrony between paired regions was identified by calculating the number of fire years recorded in both regions divided by the number of fire years recorded in either region over a centered 15-y period. This procedure was repeated in the 15 possible combinations of pairs of the six regions (the records for the two northernmost regions were too short and thus were not included) and summed as total fire synchrony, or SCFS (Fig. 2*E*).

A cutoff date of 1738 was chosen for all statistical analyses (see below) to ensure a minimum sample of recording sites ($n = 8$; >10%), a sufficient and commonly used percentage to characterize fire regimes in SSA (6, 7, 18, 30, 31). In addition, the time period of analysis ends in 1932, when both the earliest known effective fire suppression in SSA is evident in the fire records of the Río Negro and Neuquén regions, and a pulse of fire activity is initiated in the 1940s in the Aysén region associated with modern frontier activity and road construction (Fig. 2*A* and *SI Appendix*, Tables S1 and S3).

The annually resolved reconstructions of the SAM (Fig. 2*B*), the Southern Hemisphere temperature index (28) (Fig. 2*C*), and the SAS precipitation index (27) (Fig. 2*D*) were obtained from the paleoclimatology datasets of the National Centers for Environmental Information (https://www.ncdc.noaa.gov/data-access/paleoclimatology-data/datasets/climate-reconstruction). The SAM reconstruction was developed from tree ring records, and the temperature and precipitation reconstructions were developed from tree rings, marine and lake sediments, ice cores, documentary, coral and speleothem records (*SI Appendix*, Text ST1). Several SAM reconstructions have been developed (13, 26), all of which share some of the same proxies (e.g., tree ring chronologies) and thus are not independent reconstructions. We chose to use the SAM [based on the Marshall Index (9)] reconstruction because (*i*) the instrumental index used to build the SAM reconstruction is based on sea-level atmospheric pressure records from stations located between 40 °S and 65 °S, rather than on reanalysis data (SAM NCEP-NCAR), which has been shown to magnify the increase in the SAM signal over the past decades (9); (*ii*) the region (40–65 °S) used to build the index is more relevant to our study area than locations of proxies used in other reconstructions (13, 26); (*iii*) in the study areas, the summer season (i.e., December–February) of the SAM reconstruction is strongly correlated with summer weather, which is the key variable affecting fuel desiccation (13); and (*iv*) analyses based on an alternative SAM reconstruction [SAM-NCEP (26)] built from seasonal (December–February) indices are very similar (data not shown).

Seasonal subsets of monthly gridded precipitation and temperature (0.5 × 0.5 degrees; Climate Research Unit TS3.22; 1901–2013) data used to conduct bootstrapped correlation functions (see below) were derived for each study region as defined by the boxes in the map shown in Fig. 2*A*. The instrumental index of the SAM used was Marshall's summer (December–February) index (9), which is based on selected station pressure records for 40–65 °S over the period 1957–2013. This instrumental SAM index is strongly correlated with tree growth in SSA (26).

Statistical Analyses. We performed three analyses to examine the spatiotemporal associations between wildfire activity in SSA and variability in the SAM, precipitation, and temperature index reconstructions. First, at the regional scale, we determined interannual-scale departures from long-term mean SAM during periods of widespread fire and nonfire years in each of the study regions using superposed epoch analysis (SEA) (33) in the dplR package (40) in R (41) (*SI Appendix*, Fig. S2). For the SEA, years of widespread fire within each study area were defined as years when ≥2 trees were scarred, with a minimum of four trees capable of recording fire per site at ≥10% of sites (i.e., region-wide fire index for each of our eight regions). A 5-y window of mean SAM was centered on years of widespread (and no fire scars; *SI Appendix*, Fig. S3) fires for each of the study regions. Significance levels of the departures from the long-term mean were determined from bootstrapped 95% confidence intervals estimated from 10,000 Monte Carlo simulations (42). Modern teleconnections of the instrumental SAM index to local climate variability (mechanistically responsible for variability in wildfire activity) were examined with bootstrapped correlation functions using the bootRes package (43) relating the observed SAM and seasonal gridded climate data for each of the eight study regions (as defined by boxes in the map shown in Fig. 2*A* and *SI Appendix*, Fig. S4). The results of this first analysis were compared with those obtained from modern relationships (significant correlation; $P < 0.05$) between seasonal observations of both climate parameters and SAM and annual area burned in woody vegetation during the 1984–2008 period (results from ref. 3 and *SI Appendix*, Table S4).

Secondly, at the subcontinental scale, wavelet coherence was used to test whether fire activity and climatic parameters had similar periodicities, using the

Biwavelet package in R. Wavelet coherence, which identifies regions in time and space in which two variables covary, is especially suitable for the analysis of non-Gaussian time series, including climate and fire data (32). The Morlet continuous wavelet transform was applied, and the data were padded with 0s at each end to reduce wraparound effects (44). We plotted phase arrows indicating the direction of the correlation only when the wavelet coherence power exceeded the 90th percentile (Fig. 3). Although we found no difference in the coherence patterns compared with analyses conducted using standardized (*z*-scores) time series alone or standardized and detrended time series, before conducting wavelet analyses, we standardized time series (to *z*-scores) and removed trends and serial autocorrelation using autocorrelation functions and autoregressive moving average models (trend-free, prewhitened) using the Yue-Pilon method (45) in the zyp package in R.

Third, and also at the subcontinental scale, we used the Spearman correlation function to test the long-term (decadal-scale) relationships among the reconstructed SAM, the climate parameters, and both subcontinental fire indices (SCFA and SCFS) (Table 1). To highlight decadal-scale variability in climate-fire relationships, we used singular spectral analysis to determine the dominant periods at which variance occurred in the SCFA index (46); specifically, we used the multitaper method (47) to identify a window of 15 y as a cycle that explains significant proportions of variance in the SCFA over the 1738–1932 period (*SI Appendix*, Fig. S5). We used the 15-y window to construct a smoothed SCFA and the climate time series, as well as to build the SCFS. To ensure that the correlation coefficients computed in this third step were not influenced by changes over time in the sample depth (i.e., number of trees, sites, and regions recording fire), we computed correlation coefficients using a constant sample depth (10% of sites with fire-scarred trees) over time over the 1738–1932 period; that is, once the 10% criterion was achieved, new fire dates from recorder trees starting after 1738 were not added into the regional chronologies.

ACKNOWLEDGMENTS. We thank Nerilie Abram, Eric Oliver, and Tarik C. Gouhier for help with programming codes. This work was supported by the US National Science Foundation (Grants 0956552 and 0966472, to A.H., T.T.V., and J.P.), the Consejo Nacional de Investigaciones Científicas y Técnicas (J.P., I.A.M., and T.K.), the Agencia Nacional de Promoción Científica y Tecnológica (Grants PICT 2012-1891, to I.A.M., and PICT 2012-0949, to J.P.), the Graduate School of the University of Colorado Boulder (A.H. and J.P.), and the Center for Climate and Resilience Research (Comisión Nacional de Investigación Científica y Tecnológica/Fondo de Financiamiento de Centros de Investigación en Áreas Prioritarias/Award 15110009, M.E.G.) and Fondo Nacional de Desarrollo Científico (Grant 1171400, to M.E.G.).

1. Veblen TT, et al. (2011) Adapting to global environmental change in Patagonia: What role for disturbance ecology? *Austral Ecol* 36:891–903.
2. Johnston FH, et al. (2012) Estimated global mortality attributable to smoke from landscape fires. *Environ Health Perspect* 120:695–701.
3. Holz A, Kitzberger T, Veblen TT, Paritsis J (2012) Ecological and climatic controls of modern wildfire activity patterns across southwestern South America. *Ecosphere* 3:1–25.
4. Whitlock C, Moreno PI, Bartlein P (2007) Climatic controls of Holocene fire patterns in southern South America. *Quat Res* 68:28–36.
5. Kitzberger T, Veblen TT, Villalba R (1997) Climatic influences on fire regimes along a rain forest to xeric woodland gradient in northern Patagonia, Argentina. *J Biogeogr* 24:35–47.
6. Veblen TT, Kitzberger T, Villalba R, Donnegan J (1999) Fire history in northern Patagonia: The roles of humans and climatic variation. *Ecol Monogr* 69:47–67.
7. Mundo IA, Kitzberger T, Roig Juñent FA, Villalba R, Barrera MD (2013) Fire history in the *Araucaria araucana* forests of Argentina: Human and climate influences. *Int J Wildland Fire* 22:194–206.
8. Thompson DWJ, Solomon S (2002) Interpretation of recent Southern Hemisphere climate change. *Science* 296:895–899.
9. Marshall GJ (2003) Trends in the southern annular mode from observations and reanalyses. *J Clim* 16:4134–4143.
10. Manatsa D, Morioka Y, Behera SK, Yamagata T, Matarira CH (2013) Link between Antarctic ozone depletion and summer warming over southern Africa. *Nat Geosci* 6:934–939.
11. Gong D, Wang S (1999) Definition of Antarctic oscillation index. *Geophys Res Lett* 26:459–462.
12. Thompson DWJ, et al. (2011) Signatures of the Antarctic ozone hole in Southern Hemisphere surface climate change. *Nat Geosci* 4:741–749.
13. Abram NJ, et al. (2014) Evolution of the Southern Annular Mode during the past millennium. *Nat Clim Change* 4:564–569.
14. Garreaud RD, Vuille M, Compagnucci R, Marengo J (2009) Present-day South American climate. *Palaeogeogr Palaeoclimatol Palaeoecol* 281:180–195.
15. Sen Gupta A, England MH (2006) Coupled ocean-atmosphere-ice response to variations in the Southern Annular Mode. *J Clim* 19:4457–4486.
16. Garreaud RD (2007) Precipitation and circulation covariability in the extratropics. *J Clim* 20:4789–4797.
17. Silvestri GE, Vera CS (2003) Antarctic oscillation signal on precipitation anomalies over southeastern South America. *Geophys Res Lett* 30:2115.
18. Holz A, Veblen TT (2011) Variability in the Southern Annular Mode determines wildfire activity in Patagonia. *Geophys Res Lett* 38:L14710.
19. Trouet V, Taylor AH, Wahl ER, Skinner CN, Stephens SL (2010) Fire-climate interactions in the American West since 1400 CE. *Geophys Res Lett* 37:L04702.
20. Kitzberger T, Brown PM, Heyerdahl EK, Swetnam TW, Veblen TT (2007) Contingent Pacific-Atlantic Ocean influence on multicentury wildfire synchrony over western North America. *Proc Natl Acad Sci USA* 104:543–548.
21. Yao Q, et al. (2017) Pacific-Atlantic Ocean influence on wildfires in northeast China (1774 to 2010). *Geophys Res Lett* 44:1025–1033.
22. Abatzoglou JT, Kolden CA, Balch JK, Bradley BA (2016) Controls on interannual variability in lightning-caused fire activity in the western US. *Environ Res Lett* 11:045005.
23. Abatzoglou JT, Williams AP (2016) Impact of anthropogenic climate change on wildfire across western US forests. *Proc Natl Acad Sci USA* 113:11770–11775.
24. Taylor AH, Trouet V, Skinner CN, Stephens S (2016) Socioecological transitions trigger fire regime shifts and modulate fire-climate interactions in the Sierra Nevada, USA, 1600-2015 CE. *Proc Natl Acad Sci USA* 113:13684–13689.
25. Marlon JR, et al. (2008) Climate and human influences on global biomass burning over the past two millennia. *Nat Geosci* 1:697–702.
26. Villalba R, et al. (2012) Unusual southern Hemisphere tree growth patterns induced by changes in the Southern Annular Mode. *Nat Geosci* 5:793–798.
27. Neukom R, et al. (2010) Multi-centennial summer and winter precipitation variability in southern South America. *Geophys Res Lett* 37:L14708.
28. Neukom R, et al. (2014) Interhemispheric temperature variability over the past millennium. *Nat Clim Change* 4:362–367.
29. Power MJ, et al. (2008) Changes in fire regimes since the last glacial maximum: An assessment based on a global synthesis and analysis of charcoal data. *Clim Dyn* 30:887–907.
30. Holz A, Veblen TT (2012) Wildfire activity in rainforests in western Patagonia linked to the Southern Annular Mode. *Int J Wildland Fire* 21:114–126.
31. González ME, Veblen TT (2006) Climatic influences on fire in *Araucaria araucana-Nothofagus* forests in the Andean cordillera of south-central Chile. *Ecoscience* 13:342–350.
32. Mariani M, Fletcher MS, Holz A, Nyman P (2016) ENSO controls interannual fire activity in southeast Australia. *Geophys Res Lett* 43:10891–10900.
33. Baisan CH, Swetnam TW (1990) Fire history on a desert mountain range: Rincon Mountain Wilderness, Arizona, USA. *Can J For Res* 20:1559–1569.
34. Holz A, Veblen TT (2011) The amplifying effects of humans on fire regimes in temperate rainforests in western Patagonia. *Palaeogeogr Palaeoclimatol Palaeoecol* 311:82–92.
35. Holz A, et al. (2016) Fires: The main human impact on past environments in Patagonia? *PAGES Magazine* 2:72–73.
36. Garreaud RD, Gabriela Nicora M, Bürgesser RE, Ávila EE (2014) Lightning in western Patagonia. *J Geophys Res Atmos* 119:4471–4485.
37. Gillett NP, Fyfe JC (2013) Annular mode changes in the CMIP5 simulations. *Geophys Res Lett* 40:1189–1193.
38. Cai W, et al. (2015) ENSO and greenhouse warming. *Nat Clim Change* 5:849–859.
39. Taylor AH, Trouet V, Skinner CN (2008) Climatic influences on fire regimes in montane forests of the southern Cascades, California, USA. *Int J Wildland Fire* 17:60–71.
40. Bunn AG (2008) A dendrochronology program library in R (dplR). *Dendrochronologia* 26:115–124.
41. R Development Core Team (2016) *A Language and Environment for Statistical Computing* (R Institute for Statistical Computing, Vienna, Austria). Available at www.R-project.org.
42. Mooney CZ, Duval RD (1993) *Bootstrapping: A Nonparametric Approach to Statistical Inference*, Sage University Paper Series on Quantitative Applications to Social Sciences (SAGE Publications, Inc., Newbury Park, CA).
43. Zang C, Biondi F (2013) Dendroclimatic calibration in R: The bootRes package for response and correlation function analysis. *Dendrochronologia* 31:68–74.
44. Torrence C, Webster PJ (1999) Interdecadal changes in the ENSO–monsoon system. *J Clim* 12:2679–2690.
45. Yue S, Pilon P, Phinney B, Cavadias G (2002) The influence of autocorrelation on the ability to detect trend in hydrological series. *Hydrol Processes* 16:1807–1829.
46. Vautard R, Ghil M (1989) Singular spectrum analysis in nonlinear dynamics, with applications to paleoclimatic time series. *Physica D Nonlinear Phenom* 35:395–424.
47. Mann ME, Lees JM (1996) Robust estimation of background noise and signal detection in climatic time series. *Clim Change* 33:409–445.